# Higgs physics results at ATLAS

Rhys Owen on behalf of the ATLAS Collaboration
*Particle Physics Department, Science and Technology Facilities Council,*
*Rutherford Appleton Laboratory, Harwell Campus, Didcot, OX11 0QX, UK*

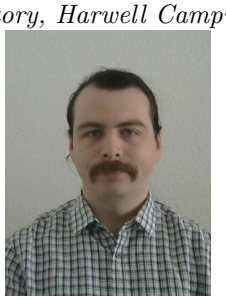

A summary of the latest Higgs results from the ATLAS detector are described. This includes measurements of $H \to b\bar{b}$ decays from VBF production, evidence for non-resonant Higgs decays to a pair of leptons and a photon ($H \to \ell\ell\gamma$), as well as the latest limits on di-Higgs production in the $b\bar{b}\gamma\gamma$ channel using the full ATLAS LHC Run-2 dataset.

ATL-PHYS-PROC-2021-028
11 May 2021

## 1 Introduction

The ATLAS collaboration[1] has a rich physics program that includes many analyses investigating Higgs boson production and decay modes using the Run-2 Large Hadron Collier (LHC) dataset. The Run-2 integrated luminosity of 139 fb$^{-1}$ represents a large increase over the 24.8 fb$^{-1}$ from Run-1 that allows ever more subtle measurements of the Higgs boson. These proceedings report on a selection of recent ATLAS results in this area.

## 2 Measurements of VBF $H \to b\bar{b}$

$H \to b\bar{b}$ is the Standard Model (SM) Higgs boson decay with the largest branching ratio, but direct measurement is experimentally challenging due to the large background of QCD interactions at the LHC.

In order to reduce these backgrounds, $H \to b\bar{b}$ is searched for in events where the Higgs boson is produced by the vector boson fusion (VBF) production mode. These recent results from ATLAS identify events associated with the VBF production mode using two different techniques; either an Adversarial Neural Network (ANN)[2] or the further requirement of an initial state radiation photon in the event are used to select the signal[3].

In this analysis, the ANN is used as a classifier in order to separate the signal events from the background contribution. The adversarial nature of the training ensures the classifier is

insensitive to $m_{b\bar{b}}$, which is the observable used to extract the signal strength from a Likelihood fit. To enhance the sensitivity of the final result, the analysis is split into ten regions depending on the pseudorapidity of the $b\bar{b}$ system and five slices of the classifier score. The insensitivity of the classifier to the mass allows events from the mass side-bands instead of simulated events to be used as the background sample in the training of the classifier. It also means the background shape is the same in all slices of the classifier value so the same parametrised background shape can be extracted from the highest statistic signal region and propagated directly to the other signal regions.

The inclusion of an additional photon in a separate analysis further suppresses the QCD background. The photon requirement also allows additional events to be selected by a trigger requiring a single photon at level 1 and then 4 jets or 3 jets and a b-jet in the higher level trigger. Background events are rejected using a Boosted Decision Tree (BDT). The classifier is trained using a Monte Carlo (MC) background samples in this analysis. However, to improve the modelling the MC samples are reweighed to match the distributions observed in the mass side bands. Three regions are then defined using the classifier output, and a likelihood fit is performed to the $m_{b\bar{b}}$ distribution.

Figure 1 shows the $m_{b\bar{b}}$ distribution for both analyses after background subtraction. As the selection criteria used in both analyses are orthogonal, they can be combined in order to extend the statistical power of the measurement. The combined signal strength is $\mu_{VBF} = 0.99^{+0.30}_{-0.30}(Stat.)^{+0.18}_{-0.16}(Syst.)$. This result represents an observed (expected) significance of 2.9 (2.9)$\sigma$ over the null hypothesis, meaning this channel is approaching a significant detection.

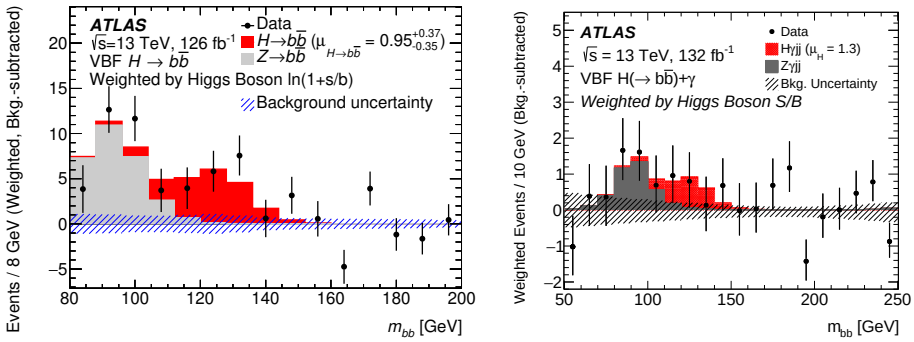


Figure 1 – Summary plots showing the results for the ANN (left)[2] and $H \to b\bar{b}\gamma$ analyses (right)[3]. Each plot is the sum of the respective signal regions weighted by their significance. The QCD background estimate is subtracted leaving the fitted $Z \to b\bar{b}$ or $Z \to jj\gamma$ component and the best fit for the signal.

## 3 Resonant and non-resonant searches for $H \to \ell\ell\gamma$

One avenue for probing the nature of the discovered Higgs boson is investigating rarer decay modes such as the decays to a pair of leptons and a photon. This decay mode is explored in the following for the case in which the two leptons form a resonance ($H \to Z\gamma \to \ell\ell\gamma$)[4] and for the non-resonant case with $m_{\ell\ell} < 30$ GeV[5].

One particularly challenging aspect of the non-resonant analysis is that for $m_{ee} < 1$ GeV, there is a high probability that the electron showers will not be well separated in the calorimeter, meaning that there is a drop in efficiency when using the conventional electron reconstruction algorithms. A dedicated merged-$ee$ reconstruction is used to recover efficiency for these events.

Events are further classified by lepton type (keeping merged-$ee$ events separate) and a kinematic classification of the event in to three categories: $VBF$-enriched, High $p_{\mathrm{Tt}}$ or Low $p_{\mathrm{Tt}}$. The quantity $p_{\mathrm{Tt}}$, defined as $p_{\mathrm{Tt}} = |\vec{p}_{\mathrm{T}}^{\,\ell\ell\gamma} \times \hat{t}|, \hat{t} = (\vec{p}_{\mathrm{T}}^{\,\ell\ell} - \vec{p}_{\mathrm{T}}^{\,\gamma})/|\vec{p}_{\mathrm{T}}^{\,\ell\ell} - \vec{p}_{\mathrm{T}}^{\,\gamma}|$ , is used instead of $p_{\mathrm{T}}^{\ell\ell\gamma}$ as it shows better experimental resolution by being less sensitive to $p_{\mathrm{T}}$ systematic uncertainties[6].

The final signal strength is determined from a simultaneous fit to all of the categories. In these fits, the signal is parametrised from Double-Sided Crystal Ball fit to Monte Carlo, and the background distribution is parametrised by either an exponential function, exponential of a second order polynomial, or a power law function. The particular function is selected to minimise bias in each separate category. These categories are summed, weighted by their sensitivity, and shown in Figure 2 (left).

The final fit provides a signal strength parameter strength of $\mu = 1.5 \pm 0.5$ compared to the SM expectation. This represents a significance of $3.2\sigma$ over the background only hypothesis ($2.1\sigma$ expected) and is the first evidence of Higgs boson decays to this final state.

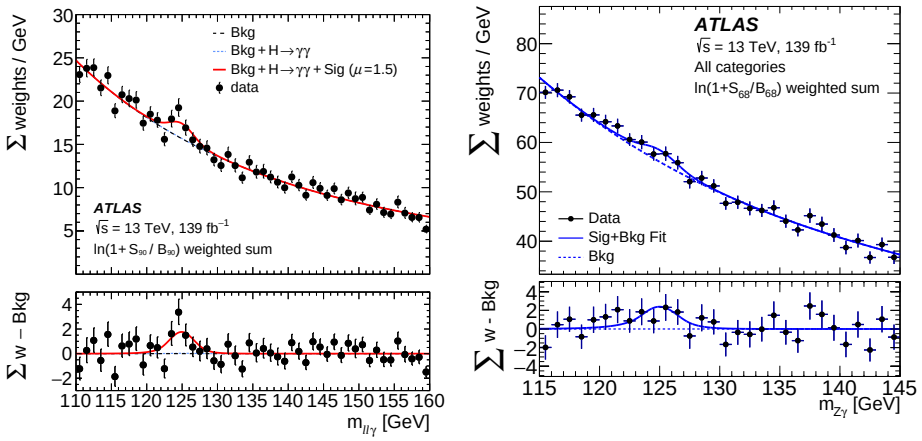


Figure 2 – Summary plots showing the results for the non resonant evidence of $H \to \ell\ell\gamma$ (left) [5] and resonant search for $H \to Z\gamma$ (right) [4]. Each plot is the sum of the respective signal regions weighted by their significance.

A similar final state in which rare Higgs decays may be detected is $H \to Z\gamma$ where the $Z$ boson is decaying leptonically. The analysis imposes similar lepton requirements to $\ell\ell\gamma$ but instead requiring $|92.1 - m_{\ell\ell}| < 10$ GeV and no merged–$ee$ category is necessary. There is, however, an additional requirement on the relative $p_{\mathrm{T}}$ of the photon and the mass of the system, $p_{\mathrm{T}}^{\gamma}/m_{Z\gamma} > 0.12$. The resulting selected events are shown with the fitted background and signal components in Figure 2 (right).

In this case, a 95% CL limit on the signal strength is set at 3.6 times the SM prediction, with expected limits of 1.7 or 2.6 for a null hypotheses excluding or including the SM Higgs production. More data is needed for conclusive evidence in this channel.

## 4 Search for di-Higgs production in the $HH \to b\bar{b}\gamma\gamma$ channel

Di-Higgs production is a rare process in the SM. The latest search results from ATLAS were obtained using the $HH \to b\bar{b}\gamma\gamma$ final state, which benefits from both the high SM branching ratio of $H \to b\bar{b}$ and the clean $H \to \gamma\gamma$ signal[7]. This process is also sensitive to beyond the standard model (BSM) couplings and is used to perform a resonant search for the decay of $X \to HH \to b\bar{b}\gamma\gamma$.

Events for this analysis are selected requiring two photons in the detector with an invariant mass 105 GeV $< m_{\gamma\gamma} <$ 160 GeV. Further, exactly two b-tagged jets are required as well as fewer than six central jets in total. A lepton veto is also included, which along with the limit on the number of central jets, maintains orthogonality of the event selection with respect to other di-Higgs searches.

For each event, a modified invariant mass, $m^{\star}_{b\bar{b}\gamma\gamma} = m_{b\bar{b}\gamma\gamma} - m_{b\bar{b}} - m_{\gamma\gamma} + 250$ GeV, is calculated. The use of an alternative mass definition improves the mass resolution especially for resonant $HH$ searches by providing cancellation of experimental resolution effects. This improved mass definition is also used in the non-resonant $HH$ search, to define low and high mass categories in

order to measure the trilinear self-coupling strength, expressed as a ratio to the SM expectation: $\kappa_\lambda = \lambda_{HHH}/\lambda^{\mathrm{SM}}_{HHH}$.

For both the resonant and non-resonant searches, the signal regions are defined using a combination of a selection BDT and the $m^{\star}_{b\bar{b}\gamma\gamma}$ distribution. For the non-resonant search, the high and low $m^{\star}_{b\bar{b}\gamma\gamma}$ categories are used simultaneously, whereas for the resonant search a number of $m_X$ mass hypotheses are considered, with a signal window in $m^{\star}_{b\bar{b}\gamma\gamma}$ defined based on the resolution expected from simulation.

A 95% confidence limit (CL) on non-resonant $HH$ production is observed (expected) at 4.1 (5.5) times the SM prediction. This result represents an improvement over previous result by a factor of five[8]. The non-resonant search is also used to set a 95% confidence interval on $\kappa_\lambda$ of $[-1.5, 6.7]$ ($[-2.4, 7.7]$) , observed (expected).

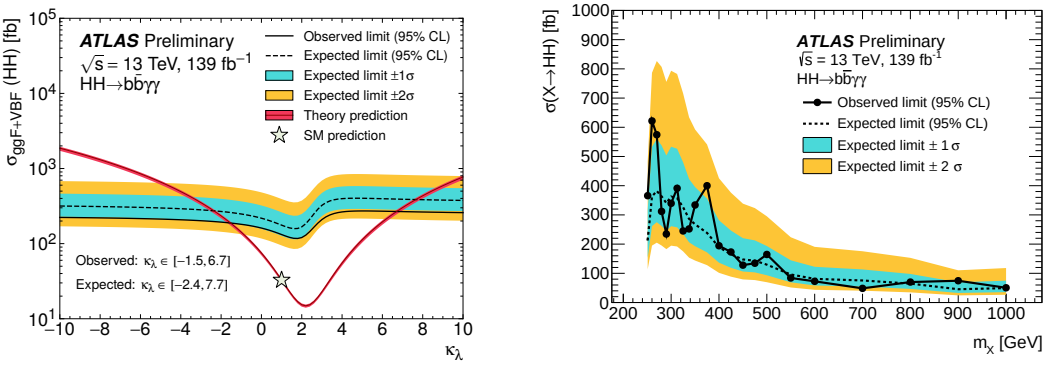


Figure 3 – Summary of limits set by the non-resonant analysis on the cross-section as a function of $\kappa_\lambda$ (left) [7] and on the resonant cross section for $X \to HH$ as a function of $m_X$ (right) [7].

Limits are set on a resonant $\sigma(X \to HH)$ for a wide range of $m_X$ from 250 GeV to 1 TeV. For the low $m_X$ region, this represents a factor of 2 improvement over the previous combined results[9]. Figure 3 summarises these results. On the left are the non-resonant limits as a function of $\kappa_\lambda$ including the theoretical prediction used to compute the confidence interval. On the right are the limit results of the individual mass points of the resonant search.

## 5 Conclusions

The ATLAS Run-2 Dataset makes it possible to study previously unobservable rare Higgs boson interactions, and these proceedings highlight some of the most recent results. Sensitivity to the VBF $H \to b\bar{b}$ production process is now at $2.9\sigma$, the first evidence is provided for Higgs boson decays to a pair of leptons and a photon, and new stricter limits on di-Higgs production and $\kappa_\lambda$ using the $HH \to b\bar{b}\gamma\gamma$ final state are obtained.

## References


1. ATLAS Collaboration. *JINST* **3**, S08003 (2008).
2. ATLAS Collaboration. [arXiv:2011.08280 [hep-ex]].
3. ATLAS Collaboration. *JHEP* **03**, 268 (2021) [arXiv:2010.13651 [hep-ex]].
4. ATLAS Collaboration. *Phys. Lett.* B **809**, 135754 (2020) [arXiv:2005.05382 [hep-ex]].
5. ATLAS Collaboration. [arXiv:2103.10322 [hep-ex]].
6. M. Vesterinen and T. R. Wyatt. *Nucl. Instrum. Methods* A **602**, 432-437 (2009).
7. ATLAS Collaboration. ATLAS-CONF-2021-016, http://cdsweb.cern.ch/record/2759683.
8. ATLAS Collaboration. *JHEP* **11**, 040 (2018). [arXiv:1807.04873 [hep-ex]].
9. ATLAS Collaboration. *Phys. Lett.* B **800**, 135103 (2020). [arXiv:1906.02025 [hep-ex]].